MOLECULAR BASIS FOR ENZYMATIC SULFITE OXIDATION – HOW THREE CONSERVED ACTIVE SITE RESIDUES SHAPE ENZYME ACTIVITY

Susan Bailey[1†]; Trevor Rapson[2]; Kayunta Johnson-Winters[3]; Andrei V. Astashkin[3]; John H. Enemark[3] and Ulrike Kappler[2]*

[1] Molecular Biophysics Group, STFC Daresbury Laboratory, Warrington, WA4 4AD, UK [2] Center for Metals in Biology, School of Molecular & Microbial Sciences, The University of Queensland, Brisbane, Qld 4072, Australia [3] Department of Chemistry, University of Arizona, Tucson, Arizona 85721, USA† Current address: Lawrence Berkeley National Laboratory, Berkeley, CA 94720, USA

Running title: Molecular basis for enzymatic sulfite oxidation

* Address correspondence to: Ulrike Kappler, Center for Metals in Biology, School of Molecular & Microbial Sciences, The University of Queensland, Brisbane, Qld 4072, Australia Phone +61 7 33652978, E-mail: u.kappler@uq.edu.au

Sulfite dehydrogenases (SDH) catalyse the oxidation and detoxification of sulfite to sulfate; a reaction critical to all forms of life. Sufite-oxidizing enzymes contain three conserved active site amino acids (Arg55, His57, Tyr236) that are crucial for catalytic competency. Here we have studied the kinetic and structural effects of two novel and one previously reported substitution (R55M, H57A, Y236F) in these residues on SDH catalysis. Both Arg55 and His57 were found to have key roles in substrate binding. An R55M substitution increased $K_{M\_sulfite\_app}$ by 2-3 orders of magnitude while His57 was required for maintaining a high substrate affinity at low pH when the imidazole ring is fully protonated. This effect may be mediated by interactions of His57 with Arg55 that stabilize the position of the Arg55 side-chain or, alternatively, may reflect changes in the protonation state of sulfite. Unlike what is seen for SDH^{WT} and SDH^{Y236F}, the catalytic turnover rates of SDH^{R55M} and SDH^{H57A} are relatively insensitive to pH (~ 60 s^{-1} and 200 s^{-1}, respectively). On the structural level striking kinetic effects appeared to correlate with disorder (in SDH^{H57A} & SDH^{Y236F}) or absence of Arg55 (SDH^{R55M}) suggesting that Arg55 and the hydrogen bonding interactions it engages in are crucial for substrate binding and catalysis. The structure of SDH^{R55M} has sulfate bound at the active site, a fact that coincides with a significant increase in the inhibitory effect of sulfate in SDH^{R55M}. Thus Arg55 also appears to be involved in enabling discrimination between the substrate and product in SDH.

Sulfite-oxidizing enzymes protect cells against potentially fatal damage to DNA and proteins caused by exposure to sulfite, and consequently they are found in all forms of life (1). In bacteria, sulfite oxidation is often linked to energy generating processes during chemolithotrophic growth on reduced sulfur compounds (2,3) while both plant and vertebrate sulfite oxidases have been shown to detoxify sulfite arising from the degradation of methionine and cysteine and exposure to sulfur dioxide (4,5).

All known sulfite-oxidizing enzymes belong to the same family of mononuclear molybdenum enzymes. Their active sites contain one molybdopterin unit per Mo atom and these enzymes may also contain heme groups as accessory redox centers (6-9). Examples of different types of sulfite-oxidizing molybdoenzymes are the homodimeric plant sulfite oxidase (PSO) which does not contain a heme group and uses oxygen as its preferred electron acceptor (9), the homodimeric chicken and human liver sulfite oxidases (CSO & HSO) (10), which are also able to use oxygen as an electron acceptor, and the bacterial sulfite dehydrogenase (SDH) isolated from the soil bacterium *Starkeya novella* (11,12) which cannot donate electrons directly to oxygen. Each monomer of CSO and HSO contains a heme *b* center in addition to the Mo center, and the redox centers are located within separate, flexibly linked domains of the same protein subunit. In contrast, the bacterial enzyme is a heterodimer where each subunit of the enzyme contains one redox center. The molybdopterin cofactor is located in the larger 40.2 kDa SorA subunit and the *c*-type heme in the smaller, 8.8 kDa SorB subunit (12). The SDH quaternary structure thus differs clearly from that of the human and chicken sulfite oxidases.

Crystal structures are available for PSO, CSO and the bacterial SDH (10,11,13-15), and have revealed molecular details of the sulfite-oxidizing enzymes. In the CSO structure the mobile heme *b* domain occupies a position too removed from the

Mo active site to mediate efficient electron transfer (10) and indeed the kinetics of this enzyme are known to be complicated by domain movements (16). In contrast, the bacterial SDH is a tight complex with strong electrostatic interactions between the subunits and the close approach of the redox centers (Mo-Fe distance 16.6 Å) allows for rapid electron transfer (11,17) (Fig. 1A,1B).

Despite the overall structural differences of these proteins, the coordination geometries of the Mo active sites of these sulfite-oxidizing enzymes are nearly identical. The oxidized molybdenum center has a square pyramidal conformation, with three sulfur and two oxo ligands (18). Within this Mo center, the equatorial oxo-ligand is proposed to be catalytically active, while the axial oxo ligand is not thought to participate directly in the reaction (Fig. 1C). During catalysis the equatorial oxo ligand is transformed into a hydroxyo/water ligand as a result of the reduction of the Mo center (Fig. 2), and it is in this form that it is generally observed in the CSO and SDH crystal structures.

SDH, CSO and HSO show similarly high affinities for their substrate, sulfite, and several highly conserved residues surround the substrate-binding and Mo-active site, namely Tyr236 (all residues given in SDH numbering, (11)), Arg55 and His57 (Fig. 1D). Both Arg55 and Tyr236 form hydrogen bonds to the catalytically active equatorial Mo-oxo group while His57 is positioned close to both Arg55 and Tyr236 (10,11) (Fig. 1D). In addition, the crystal structure of the bacterial SDH shows that Arg55 interacts directly with the second SDH redox center by hydrogen bonding to heme propionate-6 (Fig. 1D) (11).

As a result of the similarities in catalytic parameters and the structure of the active site, the bacterial SDH is a very good system for studies of enzymatic sulfite oxidation and especially the molecular basis for catalysis. As this enzyme does not rely on domain movement for catalysis, it has a less complicated reaction mechanism than the vertebrate enzymes which facilitates the interpretation of kinetic data, and it can be readily crystallized with both redox centers present in an electron transfer competent conformation. We have previously reported data on the structure, kinetics, EPR and redox properties of a Y236F substituted SDH (13). In addition to reduced turnover and substrate affinity, this substitution influences the reactivity of the SDH towards oxygen, turning SDH^{Y236F} essentially into an (albeit weak) sulfite oxidase. In order to further understand the roles of the conserved amino acids surrounding the Mo active site of sulfite-oxidizing enzymes, we have created two novel amino acid substitutions in the Arg55 and His57 residues present at the active site and have investigated their effect on catalytic and spectroscopic parameters of the bacterial SDH. We have also solved the crystal structures of the substituted enzymes which have provided new insights into the conformation and plasticity of the active site of sulfite-oxidizing enzymes and how the conserved active site residues contribute to sulfite oxidation.

Experimental procedures

Molecular Biology – Standard methods were used throughout (19). The amino acid substitutions were created using the Quikchange mutagenesis kit (Stratagene) according to the manufacturer's instructions and the pSorex plasmid (20) as the mutagenesis template. Primers R55Mf (gac gcc ttc ttc gtg **atg** tac cat ctc gcc ggt), R55Mr (acc ggc gag atg gta **cat** cac gaa gaa ggc gtc), H57Af (ttc ttc gtg cgc tac **gcc** ctc gcc ggt ata ccg) and H57Ar (cgg tat acc ggc gag **ggc** gta gcg cac gaa gaa) were used to create an Arg55 to Met and the His57 to Ala substitution as described in (13). The presence of the substitutions in the plasmids pSorex-R55M and pSorex-H57A was confirmed by DNA sequencing, followed by subcloning of the expression construct into pRK415 as described in (20). The pRK415-based expression constructs pRK-sorexR55M and pRK-sorexH57A were transferred into *Rhodobacter capsulatus* 37B4 Δ*dorA* (21) by conjugation as in (20). Following conjugation, the expression plasmids were extracted from *R. capsulatus* and the mutation confirmed by DNA sequencing.

Protein purification and characterization - recombinant protein was produced and purified as in (11). Metal analysis was performed by ICP-MS at the Acquire Center and the National Center for Environmental Toxicology, both at the University of Queensland. Protein determinations were carried out using the 2D Quant kit (GE Healthcare) or the BCA protein determination kit (Sigma-Aldrich, BCA-1), polyacrylamide gels were prepared according to (22). Oxygen reoxidation experiments were carried out as described in (13).

Crystallization and solution of the $SorAB^{R55M}$ and Sor^{H57A} crystal structures - Recombinant SDH^{R55M} and SDH^{H57A} were crystallized as previously described from 2.2 M ammonium sulfate, 2% PEG 200, 1 M HEPES, pH 7.4 (11) and crystals were cryo-cooled to 100 K within 5 days of setting up crystallization trials. Data were collected on

beamline 10.1 of the SRS, Daresbury Laboratory. Data were processed and scaled using Mosflm/SCALA (23) and further analysis used programs from the CCP4 suite (24). The crystal structure was refined with the program REFMAC (25) using the SDH^{WT} structure (11) (protein data bank code 2BlF) as the starting point and inspection of the model and electron density maps was carried out using the program O (26). Data collection, processing and refinement statistics are shown in Table 1. The final models comprise residues 1-373 of the SorA subunit, residues 1-81 of the SorB subunit, one molybdenum cofactor (Moco), one *c*-type heme, one or two sulfate ions and water molecules. The structures have good stereochemistry with 99.5% of the residues in the most favoured and additionally allowed regions and no residues in disallowed regions of the Ramachandran plot as defined by PROCHECK (27).

For the SDH^{R55M} structure, weighted difference Fourier maps calculated with coefficients mFobs-DFcalc showed a strong negative peak on the molybdenum atom which suggested that this atom is not fully occupied. This situation has already been observed for the SDH^{Y236F} structure (13) and the same procedure was used to estimate the molybdenum occupancy. The occupancy of the molybdenum was estimated at 50%. Further refinement with the molybdenum occupancy set appropriately resulted in a reasonable B-factor for this atom, similar to that of surrounding atoms, and no significant residual difference density. In the case of the SDH^{H57A} structure, the molybdenum appears fully occupied.

Enzyme assays – Routine enzyme assays were carried out at 25°C using 20 mM Tris-Acetate buffer pH 8, 2 mM sulfite, 0.04 mM cytochrome *c* (horse heart, Sigma C7752) and a suitable amount of sulfite dehydrogenase (0.1 to 0.2 nmol, depending on the variant studied) (12,13) using either a Hitachi UV3000 double beam spectrophotometer or a Cary 50 spectrophotometer (Varian). The reaction was started by the addition of sulfite and the reduction of cytochrome *c* was monitored at 550 nm. Both sulfite and cytochrome *c* solutions were prepared freshly each day. Studies of enzyme stability as a function of pH were conducted by preincubating a concentrated sample of purified enzyme at the specified pH value. Samples were removed from these solutions at various time intervals and enzyme activities immediately determined using the standard assay at pH 8.0. The normal timescale of an SDH assay is between 90s and 120s, the preincubation experiments were carried out for up to 15 minutes. For determination of $K_{Msulfite\ app}$ values, the amount of sulfite added to the assay was varied and sulfite concentrations between ~0.2 K_M and 10 K_M were used. All assays were carried out in triplicate. Buffer systems used were 20 mM Bis-Tris Acetate (pH 6.0 and 6.5), 20 mM Tris Acetate (pH 7.0-8.5), 20 mM glycine (pH 9.0-10.0), similar to the systems used in studies of CSO (28) and HSO (29), except for SDH^{R55M} where all buffers used were 20 mM Tris-Acetate. Very high concentrations of sulfite (>20 mM) were found to inhibit the SDH reaction. Kinetic constants were derived by direct non-linear regression using SigmaPlot 9.0 (SysStat Inc.).

The effect of sulfate on SDH activity (SDH^{WT} and SDH^{R55M}) was investigated in two ways: (1) increasing amounts of sulfate were added to standard SDH assays and the changes in reaction velocity observed; (2) to determine the effect of sulfate on $K_{M\ app\ sulfite}$ and $k_{cat\ app}$, these parameters were determined in the presence of 0, 10, 30 and 60 mM sodium sulfate as described above.

Non-steady-state parameters for the reductive half-reaction of wildtype and mutant SDH were determined on an SX18.MV Stopped Flow apparatus (Applied Photophysics) at 10ºC. The lowering of the temperature was necessary as the $k_{redheme}$ values observed for the wildtype enzyme were approaching the detection limits of the apparatus. Experiments were carried out using 20 mM buffers and a final conc. of 1.1 µM purified, oxidized sulfite dehydrogenase (except for SDH^{H57A} where a 0.4 µM enzyme solution was used), the reaction was monitored at 418 nm. Sulfite concentrations were varied between 2.5 and 16000 µM (final conc.) as appropriate for each enzyme used. Parameters for SDH^{Y236F} could not be determined as this enzyme can be reoxidized by molecular oxygen and accessories for anaerobic work were not available. Similarly, only a core data set could be determined for SDH^{H57A} due to the scarcity of the protein. $K_{Dsulfite}$ and $k_{red\ heme}$ were determined by direct non-linear fitting of the data.

Electron Paramagnetic resonance (EPR) –EPR samples for SDH^{WT} and SDH^{R55M} were prepared in buffers containing 100 mM Bis-Tris propane pH 7.0, whilst the SDH^{H57A} sample was prepared in 100 mM Bis-tris (pH 5.8). The pH of the buffer was adjusted using NaOH or acetic acid to give the required pH. Approximately one milligram of protein was reduced with a 20-fold excess of sodium sulfite and immediately frozen in liquid nitrogen. The continuous wave EPR spectra were recorded on a Bruker ESP-300E spectrometer at

77 K using the experimental parameters given in the legend for Figure 4. Pulsed electron-nuclear double resonance (ENDOR) experiments were performed on a homebuilt K_a-band (26-40 GHz) pulsed EPR spectrometer (30).

PDB accession codes The coordinates and structure factors of the R55M and H57A substituted SDH have been deposited with the Brookhaven protein data base with accession codes 2CA3 and 2CA4, respectively.

Results

Catalytic properties of the wildtype sulfite dehydrogenase To date, only catalytic parameters determined at pH 8 and pH 6 have been reported for SDH^{WT} (13). In order to be able to fully assess the impact of substitutions of active site amino acids on the SDH-catalyzed reaction (Fig. 2), we first determined a complete set of $K_{Msulfite\ app}$ and $k_{cat\ app}$ values for SDH^{WT} between pH 6 and 10 (Table 2, Fig. 3).

To ensure that observations made were not due to artefacts caused by inactivation of the sulfite dehydrogenase on exposure to extreme pH values, the stability of the wildtype and mutant enzymes was determined between pH 6 and 10 as a function of time. No significant loss of activity was observed (Table S1).

The apparent $K_{Msulfite}$ values for SDH^{WT} decrease with decreasing pH to a value of 0.0006 mM at pH 6, and increase markedly above pH 8.5 to a maximum of 3.4 mM at pH 10. A similar behaviour with strong increases of $K_{Msulfite\ app}$ above pH 8.5 has been reported for both CSO [$K_{Msulfite}$ 0.01 – 0.118 mM, pH 6-10] (28) and HSO [$K_{Msulfite}$ 0.0012 – 0.067 mM, pH 6-10] (29). The change in $K_{Msulfite\ app}$ seen in SDH^{WT} at higher pH values, however, is more than one order of magnitude larger than that seen for the two vertebrate enzymes. This characteristic change in substrate affinity at higher pH has been suggested to be indicative of a preference of the enzyme for hydrogensulfite (29), HSO_3^-, which has a pKa value of pH 7.2 (31). At pH 8.5 and higher, the protonated form of the substrate molecule can be expected to be present in only very small amounts (Fig. 3A).

The $k_{cat\ app}$ values for SDH increase up to pH 9.0 where a value of 519 ± 11 s^{-1} is reached, after which turnover numbers decline rapidly towards 23.7 ± 1.3 s^{-1} at pH 10 (Table 2, Fig. 3C). CSO exhibits the same behaviour with $k_{cat\ app}$ increasing up to 119 s^{-1} at pH 9.0 (28), however, HSO $k_{cat\ app}$ showed only a single pKa at low pH, and reached a steady maximal value of ~ 25 s^{-1} at pH 7.5 and higher (29).

The data in Table 2 were fitted to a bell shaped profile as described in (13) and pKa values of pH 7.5 and pH 9.7 were derived. These pKa values are slightly different from previously reported values obtained under standard assay conditions (2 mM sulfite), where maximal SDH activity is observed at pH 8.0 to 8.5 with apparent pKa values of pH 7.6 and pH 9.4 (12,13) (Fig. S1). The new data presented here clearly show that the strong increase in $K_{Msulfite\ app}$ above pH 8.5 shapes the activity profile and causes the apparent decrease in activity previously observed under standard conditions, since sulfite is no longer present in saturating concentrations.

As judged by the magnitude of the second order rate constants, SDH is a highly efficient enzyme that operates close to the limits imposed by substrate diffusion, with apparent $k_{cat}/K_{Msulfite\ app}$ values in the range of 10^7 $M^{-1}s^{-1}$ at pH 8.0 and below (Table 2, Fig. 3E). Plots of $k_{cat}/K_{Msulfite\ app}$ vs. pH have an S-shaped profile with a pKa of pH 7.0 ± 0.14.

Catalytic properties of Y236F substituted sulfite dehydrogenase – Three crucial and strictly conserved residues, Tyr236, Arg55 and His57 are found close to the Mo active site of sulfite-oxidizing enzymes and have been shown to interact with the Mo center (11,13). Tyr236 forms a hydrogen bond with the reactive equatorial oxo-group of the Mo center, an interaction that is disrupted by the Y236F substitution. We have previously reported catalytic parameters of SDH^{Y236F} at pH 6.0 and pH 8.0 (13). A full set of catalytic parameters for this enzyme is set out in Table 3. The Y236F substitution leads to an increase in $K_{Msulfite\ app}$ values by a factor of ~ 5-7. Thus, Tyr236 appears to have a moderate influence on substrate binding or the stability of the enzyme-substrate complex. This latter effect may also be mediated by changes in the ligand environment of the Mo center caused by the loss of the hydrogen bond between Tyr236 and the equatorial Mo oxo-group, although our earlier study failed to show any changes in the Mo redox potential (13). For SDH^{Y236F}, the overall shape of the $k_{cat\ app}$ vs. pH plot is similar to that seen for SDH^{WT} and the optimum pH for activity is pH 9.0 in both cases (Fig. 3D). However, in SDH^{Y236F} $k_{cat\ app}$ is lowered to about 13 % of the SDH^{WT} activity between pH 7.5 and 9.5, with SDH^{Y236F} activities at the extremes of the pH scale being matched more closely to that of SDH^{WT}. It therefore appears that in addition to its important role in

regulating the activity of sulfite-oxidizing enzymes towards oxygen (13), Tyr236 also affects enzyme turnover.

Catalytic properties of the R55M and H57A substituted sulfite dehydrogenases In order to investigate the influence of the other two strictly conserved residues on SDH activity, we created substitutions in both Arg55 and His57. The Mo content of the two novel substituted proteins was determined by ICP-MS. The Mo content of the SDH^{R55M} was between 60 and 70%, while SDH^{H57A} contained ~75-83% Mo, both being indicative of a high proportion of active enzyme in the respective preparations. As SDH^{R55M}, like the previously described SDH^{Y236F}, carries a substitution very close to the Mo active site we investigated whether the substitution of Arg55 also leads to an increased reactivity towards oxygen. However, within experimental error, the air reoxidation rates for SDH^{R55M} were the same as those determined for SDH^{WT} (13).

In steady-state assays the substitution of a Met residue for Arg55 resulted in a variant SDH characterized by two key features (Table 3): an increase of $K_{Msulfite\ app}$ by 2-3 orders of magnitude relative to SDH^{WT} and, interestingly, a nearly invariant value for $k_{cat\ app}$ (~ 65 s^{-1}) between pH 6 and pH 8. These results clearly point to an important role for Arg55 in substrate binding and/or the stabilization of the enzyme-substrate complex, as well as a role in shaping the characteristic SDH activity profile via influencing enzyme turnover.

The plot of $K_{Msulfite\ app}$ vs. pH still shows the characteristic steep increase at higher pH values, previously observed for SDH^{WT} and SDH^{Y236F}. However, we note that care should be taken in the interpretation of the higher pH catalytic data for SDH^{R55M} as these could not be reliably determined above pH 8 due to the large amounts of sulfite needed to saturate the reaction (around 10 mM at pH 6 and well over 35 mM at pH 8). Also, as a result of the large values for $K_{Msulfite\ app.}$ SDH^{R55M} appears to gain activity at lower pH values when assayed under standard conditions with 2 mM sulfite present, resulting in an activity profile with a single apparent pKa and maximal activity at pH 6 or below (Fig. S1).

Compared to SDH^{R55M} the changes in the catalytic parameters seen following a H57A substitution were more subtle (Table 3). The $k_{cat\ app}$ values were found to be fairly constant over the pH range 6-9, although SDH^{H57A} showed a higher level of activity at ~ 200 s^{-1} than SDH^{Y236F} and SDH^{R55M} over the pH ranges measured. Indeed, at pH 7 and below SDH^{H57A} $k_{cat\ app}$ rates are higher than those of the wild-type enzyme.

Substitution of His57 with alanine also lowers substrate affinity as demonstrated by the increase in $K_{Msulfite\ app}$ values. The most notable observation, however, was that the pH profile for $K_{Msulfite\ app}$ reaches a minimum at pH 7 (0.189±0.001 mM), and values increase clearly below that pH to a value of 0.667±0.12 mM at pH 6. At pH 8 and above, $K_{Msulfite\ app}$ was increased slightly (by factors of ~5-10) relative to SDH^{WT}, indicating that although it is removed from the Mo center, His57 has a role in substrate binding. None of the wild type and substituted sulfite-oxidizing enzymes (both SDH and CSO/HSO type) studied to date show a similar increase of $K_{Msulfite\ app}$ at low pH, making SDH^{H57A} a unique target for further studies into catalysis in these enzymes. Our data suggest that the protonation of the His57 residue (pKa ~6.04) (32) at lower pH values may have a major role in maintaining the high affinity of sulfite-oxidizing enzymes for sulfite (or hydrogen sulfite) at pH values below 7.

Non-steady state parameters of the reductive half-reaction of SDH – pH –dependent changes in steady state kinetic parameters may not always directly reflect a change in the molecular properties of the enzyme under study. To ascertain whether this was the case here, the non-steady state parameters for the reductive half reaction of SDH^{WT}, SDH^{R55M} and SDH^{H57A} were determined (Table 4, Fig. S2). All experiments were carried out at 10 ºC to keep reaction rates well within the specification of the instrument used.

For SDH^{WT} $K_{d\ sulfite}$ decreased with decreasing pH in the same way as the $K_{Msulfite\ app}$ values determined in steady state assays. Overall, $K_{d\ sulfite}$ values were slightly higher than the corresponding apparent $K_{Msulfite}$ values, which may be due to the different temperatures at which the assays were carried out (Table 4). In contrast, $k_{red\ heme}$ which reflects the SDH reaction rate up to the formation of the stable, Mo(V)Fe(II), two electron reduced form of SDH was nearly invariant with pH up to pH 9 at ~ 740 s^{-1}, which differs from the behaviour observed for k_{cat} but is similar to what has been reported for vertebrate sulfite oxidases (28,29). As already pointed out for CSO (28), the difference in the behaviour of k_{cat} and $k_{red\ heme}$ indicates that processes unrelated to the reductive half-reaction contribute to the kinetic barrier to catalysis. Interestingly, for both SDH^{R55M} and SDH^{H57A} a nearly pH-invariant k_{cat} similar to the SDH^{WT} $K_{d\ sulfite}$ profile.

A close correlation between the behaviour of the steady-state kinetic parameters and $K_{d\ sulfite}$ was also observed for both SDH^{R55M} and SDH^{H57A} (Table 4, Fig. S2). Due to the very low affinity of SDH^{R55M} for the substrate, sulfite, meaningful data could only be determined at pH 5.5 and 6, with the pH 7 data set clearly demonstrating the extreme increase in $K_{d\ sulfite}$ at that pH.

Only limited data could be collected for SDH^{H57A} as preparations of this protein yield much less enzyme than those of either SDH^{R55M} or SDH^{WT}. However, a plot of reaction rates versus sulfite concentrations at different pH values clearly shows that, similar to what was observed with the apparent $K_{Msulfite}$ values for this enzyme, $K_{d\ sulfite}$ reaches a minimum at pH 7.

These observations strongly suggest that the kinetic effects observed in the substituted SDH proteins are a direct result of the pH dependence of elementary steps in the enzyme's mechanism.

Characterization of the Mo centers of SDH^{R55M} and SDH^{H57A} -

The X-band CW-EPR spectra for SDH^{R55M} and SDH^{H57A} are shown in Fig. 4. For SDH^{R55M} (trace 2) the principal g-values: (g_X, g_Y, g_Z) = (1.951, 1.960, 1.989) are similar to those for SDH^{WT}: (g_X, g_Y, g_Z) = (1.9541, 1.9661, 1.9914) (12,13). For SDH^{H57A} at low pH (trace 1) the spectrum shows a well defined low-field turning point (g_Z = 1.987), but the intermediate- and high-field regions are each split into two components. One explanation of these features is to attribute them to two structurally different Mo(V) centers with different principal *g*-values. On the other hand, since the amplitudes of these components are similar, the question may arise whether they result from hyperfine splittings at g_X and g_Y. It is easy to distinguish between these two possibilities by recording an EPR spectrum at a different mw band in order to see if the positions of the EPR features scale in proportion with the mw frequency. Such measurements were performed at the mw K_a-band (~30 GHz, Fig. S3), and it was established that the EPR spectral features belong to two species, I and II, with different sets of principal g-values: (g_X, g_Y, g_Z) = (1.950, 1.962, 1.987) and (g_X, g_Y, g_Z) = (1.946, 1.959, 1.987), respectively, with g_Z being the same for both centers.

The g-values of Species I are similar to those of high pH *(hpH)* SO or SDH^{WT} (33), but the second set is somewhat different, and the question arises whether this change could be caused by some alteration of the exchangeable equatorial ligand in Species II. In order to answer this question, pulsed electron-nuclear double resonance (ENDOR) measurements at different EPR positions were performed (Fig. S4). The ENDOR spectra obtained (Fig. S4) exhibit broad shoulders with a splitting of up to 8 MHz, centered about the central sharp peaks. These shoulders were shown to arise from the OH ligand proton in the *hpH* form of sulfite-oxidizing enzymes (34). Thus, the current ENDOR measurements (Fig. S4) have shown that the characteristic features of an equatorial OH-ligand proton are present with unchanged amplitude even at the highest-field turning point that is solely contributed by Species II. This observation means that the exchangeable equatorial ligand is the same for both Species, and that it is unlikely to be responsible for the variability of the principal g-values. Rather, the interactions of Species I and II of SDH^{H57A} with the active site surroundings somehow perturb the d-orbitals of Mo(V) slightly differently. The individual structures giving rise to species I and II are likely to be very similar to one another. However, the overlap of their signals makes it impossible to investigate them separately by pulsed EPR.

Structure of SDH^{R55M} - The Arg55 side-chain of SDH^{WT} occupies an important position close to the substrate binding site, where it makes hydrogen bonds to the equatorial oxo ligand of the molybdenum, to Gln33 OE1 and a nearby water molecule. It also forms a salt-bridge, comprising two hydrogen bonds, with propionate-6 of the heme moiety of the cytochrome subunit (Fig. 1D), which effectively locks the propionate group into position (11). The guanidinium group of Arg55 stacks against the imidazole ring of His57, potentially forming a long hydrogen bond (3.5 Å) and is also found in proximity (3.8 Å) to Tyr236.

In the crystal structure of SDH^{R55M} the side-chain of Met55 does not occupy the same position as Arg55 in the SDH^{WT} structure; instead it is bent away, packing into a small cavity between the side-chains of Leu121 and Gln33. The space occupied by Arg55 in the wild-type enzyme appears to be largely empty in SDH^{R55M} and a water molecule that is hydrogen bonded to Arg55 in SDH^{WT} and is in a position to interact with the substrate/product is missing in SDH^{R55M} (Fig. 5 A,B). A small movement of the Gln33 side-chain causing a 1.0 Å shift in the position of the Gln33 OE1 may be due either to the loss of interaction with Arg55, to the position of Met55, which is located 3.0 Å from Gln33 OE1 and potentially forms an S – O hydrogen bond, or to the loss of the water molecule associated with Arg55.

In SDH^{R55M} the interactions with the heme propionate-6 moiety are also disrupted, and as a result the propionate displays greater mobility confirming our earlier suggestions that Arg55 contributes to the positioning of the propionate-6 moiety (11). Propionate-6 has been modelled in two conformations with approximately 70% of this group remaining in the same position as in SDH^{WT} and approximately 30% rotated around the C3D-CAD bond, displacing a nearby water molecule (Fig. 5).

Structure of SDH^{H57A} - The His57 side-chain of SDH^{WT} is positioned at the side of the substrate binding site between the side chains of Arg55 and Tyr236 with His57 NE2 forming a hydrogen bond to Tyr236 OH. His57 also contributes to the molybdopterin binding site via a hydrogen bond from His57 ND1 to molybdopterin O4 (11,13 and Fig. 1D).

The structure of SDH^{H57A} confirms the substitution of His57 with the smaller alanine and identifies an additional water molecule which sits close to the position occupied by the imidazole ring in SDH^{WT}. This water is at a distance to form hydrogen bonds with both N5 and O4 of the molybdopterin. In contrast with the SDH^{Y236F} and SDH^{R55M} active site mutants of SDH, the molybdenum site is fully occupied, probably reflecting the more distant position of His57 from the Mo center and the absence of a direct link to a molybdenum ligand. One consequence of the H57A substitution indicated by the difference electron density, appears to be increased mobility of both the Arg55 side-chain and the interacting propionate-6 side chain of the heme. These latter side-chains have both been modelled in two alternative conformations in this structure, approximately 65% is in the same position as in SDH^{WT} while 35% occupies an alternative position in which the salt bridge is disrupted (Fig. 5C, Fig. S5). These two alternative conformations may also account for the two different EPR signals for SDH^{H57A} (Fig. 4, see above).

The data, together with the structure of SDH^{Y236F}, reveal that both Tyr236 and His57 are necessary to stabilise Arg55 in a position for optimal hydrogen bonding to the heme 6-propionate.

Presence of sulfate in the SDH active site - Although sulfate is known to inhibit the catalytic activity of SDH and despite the fact that the crystallisation medium contained 2.2 M sulfate in all cases, sulfate it is not seen in the active sites of SDH^{WT}, SDH^{Y236F} or SDH^{H57A} (11,13). However, sulfate is present in the active site of SDH^{R55M} where it appears to displace the equatorial water/hydroxo ligand of the molybdenum as well as three solvent molecules that occupy the substrate-binding site in the wild-type structure (Figures 5&6). The sulfate anion interacts with Tyr236 OH (2.7 Å), Arg109 (2 hydrogen bonds, 2.8 Å to NH1 and 2.9 Å to NH2), the main chain N of Gly106 (2.9 Å), Cys104 Sγ (3.0 Å) and 2 water molecules (2.5 and 2.7 Å). One of the sulfate oxygen atoms is close to the position occupied by the equatorial water/hydroxo ligand in the SDH^{WT} structure, but the 3 Å distance from the molybdenum is too long for a direct Mo-sulfate/sulfite bond.

Sulfate is found in the substrate binding site of all reported CSO crystal structures (10,14). Although the position of sulfate in CSO is similar to that of the sulfate seen in SDH^{R55M}, of significant difference is that the equatorial oxygen on the Mo center is still present in the CSO structures, and the sulfate is rotated with respect to the sulfate in SDH^{R55M} so that none of the oxygen atoms is directed towards the molybdenum (Fig.6). The presence of sulfate in the active site of SDH^{R55M} could be indicative of an increased inhibition of this enzyme by sulfate, and we explored this possibility by carrying out sulfate inhibition experiments with SDH^{WT} and SDH^{R55M}. As $K_{Msulfite\ app}$ for SDH^{R55M} is extremely high (Table 3), investigations were carried out at pH 6 to allow easy addition of excess sulfate to the assay mixture. Using standard assay conditions, increasing amounts of sodium sulfate (maximum: 80 mM) were added to the reaction mixture. For SDH^{WT}, plots of the reaction velocity vs. the amount of sulfate present clearly show an exponential decay, with 50% inhibition occurring at an $I_{0.5\ pH6}$ of 22.79 mM. In contrast, for SDH^{R55M}, the observed decrease of activity with increasing amounts of sulfate was much more linear and could be fitted equally well with a linear equation or an exponential equation. An $I_{0.5\ pH6}$ value of 36.65 mM could be deduced from the exponential data fit. From this data it appears as if SDH^{R55M} is in fact slightly less susceptible to sulfate inhibition than SDH^{WT}. However, this can be shown to be not necessarily true if the concentration of sulfate necessary to achieve 50% inhibition is expressed in terms of 'excess over $K_{Msulfite\ app}$': For SDH^{WT}, 22.79 mM sulfate correspond to ~ 5.7×10^4 times $K_{Msulfite\ app}$, while for SDH^{R55M}, 36.65 mM sulfate correspond to only about 40 times $K_{Msulfite\ app}$ of this enzyme – a difference of 3 orders of magnitude, that clearly shows the higher susceptibility of SDH^{R55M} to inhibition by sulfate. Inhibition of both SDH^{WT}

and SDH^{R55M} by sulfate at pH 6 was investigated further by deriving the kinetic parameters for each enzyme at 0, 10, 30, and 60 mM sulfate present in the assay (data not shown). Analysis of this data revealed complex non-linear responses in the inhibition that indicate the potential presence of multiple binding sites for sulfate as well as a pH dependent change in the strength and type of the prevalent inhibition that is beyond the scope of this paper to discuss in detail.

Discussion

Although enzymatic sulfite oxidation has been studied for more than 4 decades, the molecular details of this process are still not well understood. In all enzymatic catalysis, the formation of the enzyme-substrate complex and the break-down of this complex into the reaction products are critical parameters, and our data presented above show for the first time how the three conserved active site residues Tyr236, Arg55 and His57 shape the activity of sulfite-oxidizing enzymes by influencing these processes. Our data suggest that crucial factors in these processes are maintaining an optimal alignment of the active site environment and possibly facilitating electron transfer between the Mo and heme redox centers (11,13).

Both Tyr236 and Arg55 are within Van der Waals contact distance of the Mo center and are hydrogen bonded to the reactive equatorial oxo/hydroxo/water ligand. His57 is located slightly further from the molybdenum. In all three cases amino acid substitution led to marked changes in the alignment of the active site residues, particularly the position of the side-chain of Arg55, and in the catalytic activity of the resulting enzymes. As no changes in the ligand environment of the heme *c* group were made and crystallography revealed few conformational changes around the heme Fe atom, it is unlikely that the physical properties of this redox center have been altered as a result of the amino acid substitutions.

The kinetic data for SDH^{Y236F} suggest that Tyr236 clearly affects enzymatic turnover, as the substitution decreases the turnover number of the SDH nearly 10 fold at the pH optimum of 8-9. The turnover numbers of SDH^{R55M} are also affected negatively and are only slightly higher than those of SDH^{Y236F}, although we note that it was only possible to measure SDH^{R55M} turnover reliably up to pH ~8. We have identified a number of possible explanations for the reduction in catalytic activity that could apply to both substitutions. Firstly, these effects could be mediated by the loss of the hydrogen bond from either Tyr236 or Arg55 to the equatorial oxo-ligand of the Mo-center. It is likely that these hydrogen-bond interactions help stabilise the Mo-center in an active state since we see some loss of molybdenum in the structures of SDH^{R55M} and SDH^{Y236F}, but not in wild type or His57 substituted enzymes. Secondly, both structures identify a disruption of the salt bridge between Arg55 and heme propionate-6 which may affect electron transfer between the two redox centers, although we note that the Mo-Fe distance of 16.6 Å may be close enough to allow electron 'tunnelling' to occur (35). Finally, we cannot rule out the possibility that the reduced activity is due to changes in the redox properties of the Mo atom, although we have so far failed to find evidence for such changes (13).

It is also interesting to note that in SDH^{WT} and SDH^{Y236F}, $k_{cat\ app}$ is clearly pH-dependent in a similar manner, while in SDH^{R55M} and SDH^{H57A} $k_{cat\ app}$ values were steady from pH 6 to pH 8, with SDH^{H57A} exhibiting a single pKa in the high pH range above pH 9. As expected by its greater proximity to the Mo center, the effect of the R55M substitution on enzymatic turnover is much more severe than that of the H57A substitution, however, in both cases the pKa value at pH 7.5 seen in the SDH^{WT} $k_{cat\ app}$ values is lost. The data imply that both His57 and Arg55 have a role in defining this low pH pKa.

The R55M substitution also led to a significant increase in $K_{Msulfite\ app}$ by 2-3 orders of magnitude, which, in addition to the observed reduction in $k_{cat\ app}$ is likely exacerbated by changes in either formation rate of the enzyme-substrate complex and/or the rate at which the complex dissociates without catalysis having been achieved. These latter two effects would be specific to the R55M substitution as SDH^{Y236F} shows a similarly reduced rate of turnover while maintaining a much higher substrate affinity. The less severe increase in $K_{Msulfite\ app}$ for SDH^{Y236F} and SDH^{H57A} may be at least partially due to disturbances in the position of Arg55 since the crystal structures of both SDH^{Y236F} and SDH^{H57A} show that this residue is sensitive to its interactions with Tyr236 and His57.

An entirely different and previously unobserved change in the pH dependence of $K_{Msulfite\ app}$ occurred in SDH^{H57A}: in all wild type and substituted SDH/SO enzymes studied so far, the affinity for the substrate increases at lower pH values, but in SDH^{H57A} a minimum affinity for sulfite was reached at pH 7, indicating that His 57 is important in maintaining substrate affinity

below pH 7, where the bulk of the substrate will be present in its protonated HSO_3^- form. At pH 7 and below the His57 imidazole ring should also be fully protonated and the effect of His57 on substrate binding may be exerted through its interactions with Arg55.

Substitution of Arg55 with methionine essentially creates an open space at the center of the SDH active site and disrupts the hydrogen bond network around the Mo and connecting the molybdopterin and heme redox centers. At the same time Arg55 is also the innermost of the positively charged residues that line the active site channel of both SDH and CSO/HSO enzymes. There is evidence from the CSO structures that the arginine residues in the active site channel (Arg138/55, Arg190/109 and Arg450,-; CSO/SDH numbering) are involved in achieving the correct orientation of the incoming sulfite molecule with respect to the Mo center (10).

The crystal structure of SDH^{R55M} is the only structure of SDH (11,13) that has a sulfate molecule bound at the active site, despite the fact that the crystallization medium contains 2.2M ammonium sulfate in all cases (Fig.6). Modelling a sulfate molecule in the substrate binding site of SDH^{WT} in the same position and orientation as the sulfate in the SDH^{R55M} structure demonstrates that there is no clash with the position of the Arg55 side-chain and that two sulfate oxygen atoms are positioned to form hydrogen bonds with NE and NH2 of Arg55. However, the position and orientation of the sulfate molecule in the SDH^{R55M} active site is slightly different from that seen in the CSO structures (10) since one of the sulfate oxygen atoms is positioned facing the molybdenum active site. Although the sulfate oxygen is too distant to actually bond to the molybdenum it does appear to be able to displace the equatorial oxo/ hydroxo/water ligand of the Mo-center in the absence of Arg55. We therefore propose that Arg55 plays an important role not only in substrate binding, as demonstrated by our kinetic data, but also in product dissociation from the active site.

It is probable that the composition of the crystallization medium facilitates the formation of the sulfate complex seen in the crystal structure (Fig. 5B) which would be showing in effect a sulfate inhibited form of the SDH. It seems less likely that the loss of the equatorial oxo/hydroxo/water ligand to the Mo center seen in the crystal structure is a permanent feature of SDH^{R55M}. A complete loss of the equatorial molybdenum ligand would be expected to have much more pronounced effects on catalysis as this ligand is central to the formation of the enzyme-substrate complex. Pulsed EPR studies that are in progress, including ^{17}O labelling experiments, should provide important insight concerning the structure of the Mo(V) center of SDH^{R55M}.

It is not clear why the wild-type and other substituted SDH structures do not have sulfate bound in the active site channel. One speculative possibility is the loss of a water molecule in the SDH^{R55M} structure, which hydrogen bonds to Arg55 NH2, Glu33 OE1 and Gly119 N in the wild type enzyme. This water is in a position that would allow it to hydrogen bond to the substrate/product and we propose a possible role in enzyme activity for this water molecule which could displace the product sulfate from the molybdenum to become the water/hydroxo ligand of the reduced molybdenum redox center.

The changes seen in catalysis and the structure of SDH^{R55M} are also of interest because this substitution is related to the R160Q substitution in the human sulfite oxidase (36), which is of clinical relevance and has been identified in an SO deficiency patient (14). In HSO, Arg160 (Arg138 in CSO) likely occupies an equivalent position to that of Arg55 in SDH in the active site. Under standard assay conditions at pH 8, the $K_{Msulfite\ app}$ of HSO^{R160Q} was lowered by a factor of 100, and $k_{cat\ app}$ was decreased by ~6.7 times relative to HSO^{WT} (36). The decreases in both values are nearly identical to those reported in this paper for SDH^{R55M} suggesting that the kinetic effects of the R160Q and the R55M substitutions are quite similar. The sulfite oxidases from vertebrates are closely related, and the crystal structure of a R138Q substituted CSO was recently reported (14). The structure showed a slightly altered position of Gln138 compared with that occupied by Arg138 in CSO^{WT} and small changes in the relative positions of Tyr322 and Arg190 (equivalent to Tyr236 and Arg109 in SDH), both located in the active site channel of the vertebrate sulfite oxidases (14). The major change observed in the CSO^{R138Q} active site, however, was a pronounced change in the position of the side chain of the outermost of the three arginines, Arg450 (replaced by an alanine residue in SDH), which results in a narrowing of the active site entrance channel and was proposed to serve as a gating mechanism (14). As this gating mechanism can clearly not be functional in SDH which lacks an Arg450 equivalent, and in view of the similarity of the kinetic data for HSO^{R160Q} and

SDH^{R55M} it is unclear what influence the gating mechanism has on sulfite oxidation.

In summary, this work presents for the first time a comprehensive kinetic and structural analysis of the effect that the amino acid environment of the SO/SDH active site has on enzymatic catalysis. Substitution of Tyr236 slows down enzymatic turnover significantly while only a moderate effect on substrate affinity was observed. Our data indicate that Arg55 is the most important of the three conserved active site residues as it mediates substrate binding and product release as well as influencing turnover. SDH^{R55M} was the least catalytically competent (Fig. 3F) of the three substituted enzymes investigated here. We have also uncovered the previously unrecognized role of His57 in substrate binding and low pH catalysis. Additionally, for SDH^{H57A} the presence of two active site structural conformations and two distinct EPR forms raises the possibility of more than one catalytic pathway.

The similarity of the SDH^{R55M} data to data previously reported for HSO^{R160Q} clearly shows the applicability of SDH derived data for enzymatic sulfite oxidation in general.

References

1. Kappler, U. (2007) Bacterial sulfite dehydrogenases - enzymes for chemolithtrophs only? In: Friedrich, C. G. and Dahl, C., editors. *Microbial Sulfur Metabolism*, Springer, Berlin

2. Suzuki, I. (1994) *Methods Enzymol.* **243,** 447-454

3. Kappler, U. and Dahl, C. (2001) *FEMS Microbiol. Lett.* **203,** 1-9

4. Rajagopalan, K. V. (1980) Sulfite oxidase (Sulfite: Ferricytochrome *c* Oxidoreductase). In: Coughlan, M. P., editor. *Molybdenum and Molybdenum-Containing Enzymes*, Pergamon Press, Oxford

5. Hansch, R., Lang, C., Riebeseel, E., Lindigkeit, R., Gessler, A., Rennenberg, H., and Mendel, R. R. (2006) *J. Biol. Chem.* **281,** 6884-6888

6. Karakas, E. and Kisker, C. (2005) *Dalton Trans.* 3459-3463

7. Feng, C., Tollin, G., and Enemark, J. H. (2007) *Biochimica et Biophysica Acta (BBA) - Proteins & Proteomics* **1774,** 527-539

8. Enemark, J. H. and Cosper, M. M. (2002) *Met. Ions Biol. Syst.* **39,** 621-654

9. Mendel, R. R. and Bittner, F. (2006) *Biochim. Biophys. Acta* **1763,** 621-635

10. Kisker, C., Schindelin, H., Pacheco, A., Wehbi, W. A., Garrett, R. M., Rajagopalan, K. V., Enemark, J. H., and Rees, D. C. (1997) *Cell* **91,** 973-983

11. Kappler, U. and Bailey, S. (2005) *J. Biol. Chem.* **280,** 24999-25007

12. Kappler, U., Bennett, B., Rethmeier, J., Schwarz, G., Deutzmann, R., McEwan, A. G., and Dahl, C. (2000) *J. Biol. Chem.* **275,** 13202-13212

13. Kappler, U., Bailey, S., Feng, C. J., Honeychurch, M. J., Hanson, G. R., Bernhardt, P. V., Tollin, G., and Enemark, J. H. (2006) *Biochemistry.* **45,** 9696-9705

14. Karakas, E., Wilson, H. L., Graf, T. N., Xiang, S., Jaramillo-Buswuets, S., Rajagopalan, K. V., and Kisker, C. (2005) *J. Biol. Chem.* **280,** 33506-33515

15. Schrader, N., Fischer, K., Theis, K., Mendel, R. R., Schwarz, G., and Kisker, C. (2003) *Structure* **11,** 1251-1263

16. Feng, C. J., Kedia, R. V., Hazzard, J. T., Hurley, J. K., Tollin, G., and Enemark, J. H. (2002) *Biochemistry.* **41,** 5816-5821

17. Feng, C. J., Kappler, U., Tollin, G., and Enemark, J. H. (2003) *J. Am. Chem. Soc.* **125,** 14696-14697

18. Hille, R. (1996) *Chem. Rev.* **96,** 2757-2816

19. Ausubel, F. M., Brent, R., Kingston, R. E., Moore, D. D., Seidman, J. G., Smith, J. A., and Struhl, K. (2005) *Current Protocols in Molecular Biology*, John Wiley & Sons Inc., Hoboken, NJ

20. Kappler, U. and McEwan, A. G. (2002) *FEBS Lett.* **529,** 208-214

21. Ridge, J. P., Aguey-Zinsou, K. F., Bernhardt, P. V., Brereton, I. M., Hanson, G. R., and McEwan, A. G. (2002) *Biochemistry.* **41,** 15762-15769

22. Laemmli, U. K. (1970) *Nature* **227,** 680-685

23. Leslie, A. G. W. (1992) *Joint CCP4 and ESF-EACMB Newsletter on Protein Crystallography* **26,**

24. CCP4 (1994) *Acta Cryst.* **D10,** 760-763

25. Jones, T. A., Zou, J. Y., Cowan, S. W., and Kjeldgaard, M. (1991) *Acta Cryst.* **A47,** 110-119

26. Murshudov, G. N., Vagin, A. A., and Dodson, E. J. (1997) *Acta Cryst.* **53,** 240-255

27. Laskowski, R. A., Macarthur, M. W., Moss, D. S., and Thornton, J. M. (1993) *J. Appl. Crystallogr.* **26,** 283-291

28. Brody, M. S. and Hille, R. (1999) *Biochemistry.* **38,** 6668-6677

29. Wilson, H. L. and Rajagopalan, K. V. (2004) *J. Biol. Chem.* **279,** 15105-15113

30. Astashkin, A. V., Enemark, J. H., and Raitsimring, A. M. (2006) *Concepts Magn. Reson. Part B* **29B,** 125-136

31. Aylward, G. H. and Findlay, T. J. V. (1971) Dissociation constants of Acids and Hydrated Metal Ions. *SI-Chemical Data*, John Wiley & Sons,

32. Dawson, R. M. C., Elliott, D. C., Elliott, W. H., and Jones, K. M. (1969) *Data for biochemical research*, 2 Ed., Oxford University Press, Oxford

33. Enemark, J. H., Astashkin, A. V., and Raitsimring, A. M. (2006) *Dalton Trans.* 3501-3514

34. Astashkin, A. V., Raitsimring, A. M., Feng, C. J., Johnson, J. L., Rajagopalan, K. V., and Enemark, J. H. (2002) *J. Am. Chem. Soc.* **124,** 6109-6118

35. Page, C. C., Moser, C. C., Chen, X., and Dutton, L. (1999) *Nature* **402,** 47-52

36. Garrett, R. M., Johnson, J. L., Graf, T. N., Feigenbaum, A., and Rajagopalan, K. V. (1998) *Proc. Natl. Acad. Sci. U. S. A.* **95,** 6394-6398

37. DeLano, W. L. (2002) *DeLano Scientific, Palo Alto, CA, USA*

Footnotes

Acknowledgements: This work was supported by a grant and fellowship from the University of Queensland to UK, an Endeavour IPRS scholarship from the University of Queensland to TDR and by STFC Daresbury laboratory support for SB. During document preparation, SB was supported by the Director, Office of Science, Office of Basic Energy Sciences, of the U.S. Department of Energy under Contract No. DE-AC02-05CH11231. Support of the National Institutes of Health (GM-37773 to JHE and a Ruth L. Kirschstein National Service Award to KJ-W) are gratefully acknowledged. We thank Dr. A. Raitsimring for helpful discussions concerning the EPR spectra.

Figure legends:

Figure 1 – Details of the crystal structure of wild-type SDH and comparison with CSO. **A:** *Ribbon diagram of the SDH heterodimer* with the SorA and SorB subunits coloured blue and cyan respectively and the redox cofactors in space-filling mode with the molybdenum atom coloured green and the iron atom coloured violet. **B:** *Ribbon diagram of a single subunit of CSO* with the molybdopterin binding domain in the same orientation as SorA in A. The cytochrome domain of CSO is clearly in a different position with respect to the molybdenum cofactor than is seen for the cytochrome subunit of SDH. **C:** *SDH molybdopterin cofactor demonstrating the geometry of the molybdenum ligands*: the thiol ligands donated by the organic component of molybdopterin and the Cys104 side chain, and the reactive oxygen ligand (Oeq) sit in the equatorial plane with the axial oxygen (Oax) ligand at the apex of a square pyramid. (Atoms are coloured as follows: molybdenum, green; sulfur, orange; phosphorous, magenta; oxygen, red; nitrogen, blue and carbon, yellow in the cofactor and white in the protein). **D:** *Hydrogen bonding network around the substrate binding site*. The molybdopterin and heme cofactors are shown together with active site residues Cys104, Arg55, His57, Tyr236 and Gln33. Figures 1 and 4 were prepared using Pymol (37).

Figure 2 – Proposed reaction mechanism for *S. novella* sulfite dehydrogenase. The reaction is shown in terms of the redox states of the molybdenum and heme centers present in the enzyme. In bold & boxed: stable redox states of the *S. novella* SDH. "Cyt. c" denotes a mitochondrial-type cytochrome c_{550} (e.g. horse heart, or *S. novella* cytochrome c_{550}) that can act as the external electron acceptor.

Figure 3 – Influence of pH on the kinetic parameters of SDH^{WT} and its substituted forms.
Panel A: Plot of $K_{Msulfite\ app}$ for SDH^{WT} and sulfite speciation vs. pH;
Panel B: Plot of $K_{Msulfite\ app}$ vs. pH for SDH^{R55M} (×), $SDH^{Y236}F$ (•) and SDH^{H57A} (◊)
Panel C: Plot of $k_{cat\ app}$ vs. pH for SDH^{WT}
Panel D: Plot of $k_{cat\ app}$ vs. pH for SDH^{R55M} (×), $SDH^{Y236}F$ (•) and SDH^{H57A} (◊)
Panel E: Plot of $k_{cat}/K_{Msulfite}$ vs. pH SDH^{WT};
Panel F: Plot of $k_{cat}/K_{Msulfite}$ vs. pH for SDH^{R55M} (×), $SDH^{Y236}F$ (•) and SDH^{H57A} (◊)

Figure 4 – CW EPR spectra of SDH forms. Trace 1: SDH^{H57A} at pH 5.8; Trace 2: SDH^{R55M} at pH 7.0. Experimental conditions: ν_{mw} = 9.444 GHz; modulation amplitude = 0.1 mT; mw power = 0.2 mW; temperature = 77 K. The narrow line at g = 2.0036 is the signal of the DPPH standard.

Figure 5 – Active site structures of SDH^{R55M} and SDH^{H57A}. **A**. and **B.** show a transparent surface at the substrate binding sites of SDH^{WT} and SDH^{R55M} respectively. The water-filled cavity adjacent to the equatorial oxygen is larger in the mutated enzyme and is occupied by a sulfate ion. **C.** Hydrogen bonding network around the active site of SDH^{H57A} in a similar view as SDH^{WT} in Figure 1D. The two alternative positions for Arg55 and the heme propionate group are shown. An additional water molecule occupies a site close to the pterin, and fulfils potential hydrogen-bond contacts.

Figure 6 – Comparison of the position of bound sulfate in the active sites of SDH^{R55M} and CSO. The stereoview shows the two active sites superimposed with the CSO residues colored grey, and the the SDH^{R55M} atoms colored as follows: molybdenum, green; sulfur, orange; phosphorous, magenta; oxygen, red; nitrogen, blue and carbon, cyan. Labels show residues with SDH numbering.

Supplementary figures:

Figure S1– Activity (in U/mg) vs. pH profiles for SDH^{WT}, SDH^{Y236F}, SDH^{R55M}, SDH^{H57A} recorded using standard assay conditions, i.e. 2 mM sulfite and 0.04 mM cytochrome *c* (horse heart).

Figure S2 – Stopped Flow data for the reductive half reaction of SDH^{H57A} – plots of reaction rates (s^{-1}) collected at different pH values vs. sulfite concentration are shown. Filled circles (●) – pH 6, open circles (○) – pH 7, filled triangles (▼) – pH 8, open triangles (△) – pH 9. The increase in reaction rate with increasing sulfite concentrations, which is maximal for data collected at pH 7, reflects the magnitude of k_d sulfite. The data mirror the behavior of the steady-state parameter $K_{M\ sulfite\ app}$.

Figure S3 - Comparison of the X-band CW EPR (trace I) and K_a-band ESE field sweep (trace 2, numerical first derivative) of SDH^{H57A} shows that the features seen at the high-field side of the EPR spectrum are caused by the presence of centers with different g-tensors, and not by the *hfi*. Experimental conditions for trace 1: mw frequency, 9.461 GHz; mw power, 200 μW; modulation amplitude, 0.2 mT; temperature, 77 K. Experimental conditions for trace 2: mw frequency, 29.566 GHz; mw pulses, 2×80 ns (two-pulse sequence); time interval between the mw pulses, τ = 300 ns; boxcar integration gate, 150 ns; temperature, 21 K.

Figure S4 - Refocused ^{1}H Mims ENDOR spectra of SDH^{H57A} at different EPR positions, as indicated in the Figure. Experimental conditions: mw frequency, 29.566 GHz; mw pulses, 3×13 ns + 20 ns; time interval between the first two mw pulses, τ = 80 ns; time interval between the second and the third mw pulses, T = 30 μs; RF pulse length, 20 μs; stochastic RF sweep; temperature, 21 K. The bottom spectrum is recorded at the high-field side of the spectrum where only Species II with the lowest g_X is contributing. The narrow features with splittings ≤ 4 MHz in all spectra are mostly contributed to by the non-exchangeable protons belonging to the protein. The broad features with splittings > 4 MHz are characteristic of an exchangeable proton of the equatorial OH ligand (34). The broad feature under the more narrow central lines comes from the proton of the equatorial OH ligand. This shows that the Mo(V) center of Species II has essentially the same structure as that of Species I (usual *hpH*-type center).

Figure S5
Stereo views of electron density around the Mo active site showing the molybdenum cofactor surrounded by residues Arg55, His57, Cys104 and Tyr236. **A**. R55M substituted enzyme with bound sulfate contoured at 1.5s. **B**. H57A substituted enzyme demonstrating disordered R55 contoured at 1.2s. **C**. Y236F substituted enzyme demonstrating slightly disordered R55 contoured at 1.2s. **D**. Wild-type enzyme contoured at 1.5s. All maps were calculated using data to 2 Å.

Tables

Table 1 Data collection and refinement statistics

	R55M	H57A
Data collection		
Beamline	SRS 10.1	SRS 10.1
Wavelength (Å)	1.074	1.074
Resolution range (Å)	50-2.0	50-2.1
Unique reflections	34463	27649
Completeness (%)[1]	98.2 (89.1)	93.0 (83.8)
Multiplicity[1]	3.8 (2.7)	3.4 (2.0)
$I/\sigma(I)$ [1]	14.3 (3.8)	10.6 (2.1)
R_{merge}[2] (%)[1]	9.5 (28.8)	10.2 (41.8)
Refinement statistics		
Resolution range(Å)	30-2.0	20-2.1
R_{cryst}[2] (%)	16.3	14.7
R_{free}[4] (%)	20.7	20.1
R.m.s. deviations from ideal geometry		
bond lengths (Å)	0.016	0.012
rmsd bond angles	1.59	1.4
Number of water molecules	357	378

[1] Values in parentheses refer to the highest resolution shells of 2.07-2.0 Å and 2.21-2.1 Å.
[2] $R_{merge} = \Sigma_h\Sigma_i |(I_{hi} - I_h)|/ \Sigma_h\Sigma_i |(I_{hi})$.
[3] $R_{cryst} = \Sigma|F_o-F_c|/\Sigma F_o$ where F_o and F_c are the observed and calculated structure factor.
[4] R_{free} was calculated with 5% of the data that had been excluded from refinement

Table 2 Kinetic parameters of the SorAB sulfite dehydrogenase (SDH^{WT}) from *Starkeya novella*

pH	$K_{M\ sulfite}$ (mM)	k_{cat} (s^{-1})	$k_{cat}/K_{M\ sulfite}$ ($M^{-1}s^{-1}$)
6.0	$0.6 \times 10^{-3} \pm 9.5 \times 10^{-5}$	63.5 ± 2.2	1.06×10^{8}
6.5	$1.1 \times 10^{-3} \pm 0.14\ 10^{-3}$	86.2 ± 2.2	7.55×10^{7}
7.0	$3.7 \times 10^{-3} \pm 0.45\ 10^{-3}$	158.8 ± 4.5	4.27×10^{7}
7.5	$7.1 \times 10^{-3} \pm 0.82 \times 10^{-3}$	293.4 ± 7	4.03×10^{7}
8.0	$2.2 \times 10^{-2} \pm 0.26 \times 10^{-2}$	345.3 ± 11	1.53×10^{7}
8.5	$8.6 \times 10^{-2} \pm 0.85 \times 10^{-2}$	410 ± 11	4.88×10^{6}
9.0	0.324 ± 0.029	519 ± 11	1.5×10^{6}
9.5	1.66 ± 0.18	431 ± 16	2.51×10^{5}
10.0	3.389 ± 0.44	23.7 ± 1.3	6.77×10^{3}

Table 3 Kinetic parameters of substituted SorAB sulfite dehydrogenases, SDH^{Y236F}, SDH^{R55M} and SDH^{H57A}. Square brackets, [ ], denote values for which insufficient data points could be obtained due to the high sulfite concentrations needed to achieve saturating sulfite concentrations.

SDH Y236F kinetic parameters			
pH	$K_{M\ sulfite}$ (mM)	k_{cat} (s^{-1})	$k_{cat}/K_{M\ sulfite}$ ($M^{-1}s^{-1}$)
6.0	$0.004 \pm 0.6 \times 10^{-3}$	36.8 ± 1.5	8.42×10^{6}
6.5	$0.007 \pm 0.6 \times 10^{-3}$	41.6 ± 0.8	5.60×10^{6}
7.0	0.026 ± 0.0032	51.8 ± 1.5	1.97×10^{6}
7.5	0.042 ± 0.0041	48.3 ± 1	1.14×10^{6}
8.0	0.114 ± 0.0135	53.4 ± 1.6	4.61×10^{5}
8.5	0.332 ± 0.0447	58.3 ± 2.4	1.73×10^{5}
9.0	1.155 ± 0.1166	64 ± 2	5.45×10^{4}
9.5	4.456 ± 0.6693	52.7 ± 3.5	1.16×10^{4}
10.0	15.487 ± 2.8	44.8 ± 4.7	2.84×10^{3}
SDH R55M kinetic parameters			
pH	$K_{M\ sulfite}$ (mM)	k_{cat} (s^{-1})	$k_{cat}/K_{M\ sulfite}$ ($M^{-1}s^{-1}$)
5.8	0.812 ± 0.114	70.5 ± 2.4	8.68×10^{4}
6.2	1.087 ± 0.26	64.0 ± 3.9	5.89×10^{4}
6.6	1.63 ± 0.39	64.0 ± 4.3	3.93×10^{4}
7.0	1.95 ± 0.49	66.3 ± 4.2	3.4×10^{4}
7.5	3.62 ± 0.57	68.3 ± 3.3	1.89×10^{4}
7.9	8.17 ± 1.37	73.4 ± 4.8	8.98×10^{3}
8.3	[33.27 ± 7.5]	[109.88 ± 15.04]	[3.3×10^{3}]
SDH H57A kinetic parameters			
pH	$K_{M\ sulfite}$ (mM)	k_{cat} (s^{-1})	$k_{cat}/K_{M\ sulfite}$ ($M^{-1}s^{-1}$)
6.0	0.667 ± 0.12	238.8 ± 16.5	3.58×10^{5}
6.5	0.29 ± 0.003	226.5 ± 7.6	7.82×10^{5}
7.0	0.189 ± 0.001	214.5 ± 3.7	1.13×10^{6}
7.5	0.22 ± 0.002	220.5 ± 5.6	1.01×10^{6}
8.0	0.27 ± 0.003	214.6 ± 6	7.99×10^{5}
8.5	0.452 ± 0.06	222.4 ± 9.9	4.92×10^{5}
9.0	1.46 ± 0.16	192.5 ± 7.5	1.32×10^{5}
9.5	12.2 ± 3.4	148.4 ± 25.8	1.22×10^{4}

Table 4 Non-steady state kinetic parameters for the reductive half reaction of the SDH^{WT} and SDH^{R55M} sulfite dehydrogenases. Data were collected at 418 nm and 10 ºC.

SDH WT

pH	$K_{d\ sulfite}$ (mM)	k_{red} heme (s^{-1})	k_{red} heme/ $K_{d\ sulfite}$ ($M^{-1}\ s^{-1}$)
6	0.0032 ± 0.0003	730 ± 10	2.25×10^8
6.5	0.0036 ± 0.0002	847± 10	2.39×10^8
7	0.0014 ± 0.0001	782 ± 16	5.58×10^7
7.5	0.0031 ± 0.0003	677 ± 20	2.18×10^7
8	0.0087 ± 0.0007	776 ± 22	8.89×10^6
8.5	0.412 ± 0.029	829 ± 32	2.01×10^6
9	1.183 ±0.094	731 ± 20	6.18×10^5
9.5	3.811 ± 0.75	674 ± 45	1.77×10^5

SDH R55M

pH	$K_{d\ sulfite}$ (mM)	k_{red} heme (s^{-1})	k_{red} heme/ $K_{d\ sulfite}$ ($M^{-1}\ s^{-1}$)
5.5	4.53 ± 0.51	746 ± 34	1.65×10^5
6	6.48 ± 0.68	662 ± 31	1.02×10^5
7	[22.8 ± 4.5]	[240 ± 32]	[1.05×10^4]

Table S1 - Stability of SDH^{WT} following pre-incubation at different pH values. Purified SDH^{WT} was diluted into buffers of the specified pH. Three individual dilutions were set up for each pH. Samples were taken from these buffers at specified times and immediately used in standard SDH assays at pH 8.0. The data is shown as μmoles sulfite oxidized per minute in the assay. Similar data was collected for SDH^{R55M} and SDH^{H57A} at pH 6.0, 8.0 and 10.0 (data not shown) and also showed that on the timescale of a standard SDH assay (1-2 minutes) the enzyme is stable at all pH values used in this study.

Time (min)	**pH 6.0**	**pH 7.0**	**pH 8.0**	**pH 9.0**	**pH 10.0**
0	0.0162	0.0149	0.0177	0.0142	0.0152
5	0.0158	0.0146	0.0165	0.0145	0.0174
10	0.0175	0.0144	0.0183	0.0146	0.0198
15	0.0197	0.0151	0.0165	0.0144	0.0172

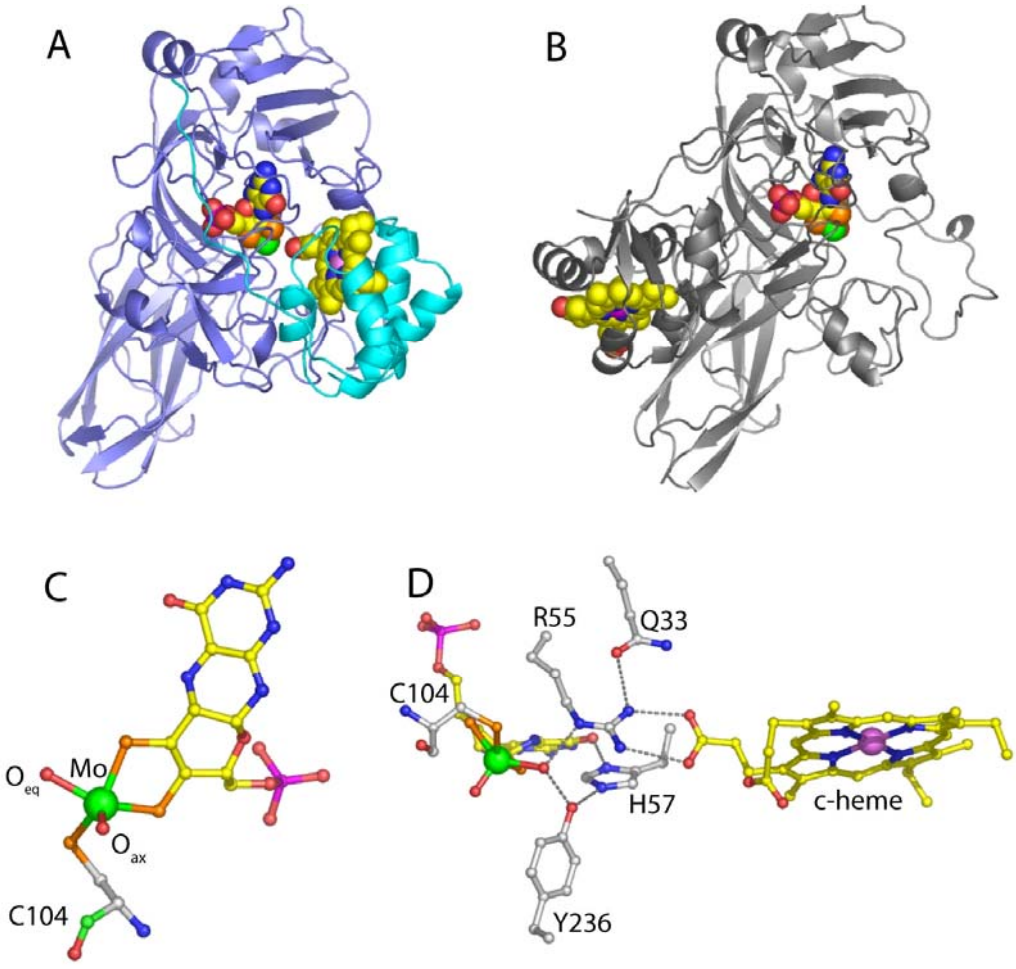

Figure 1

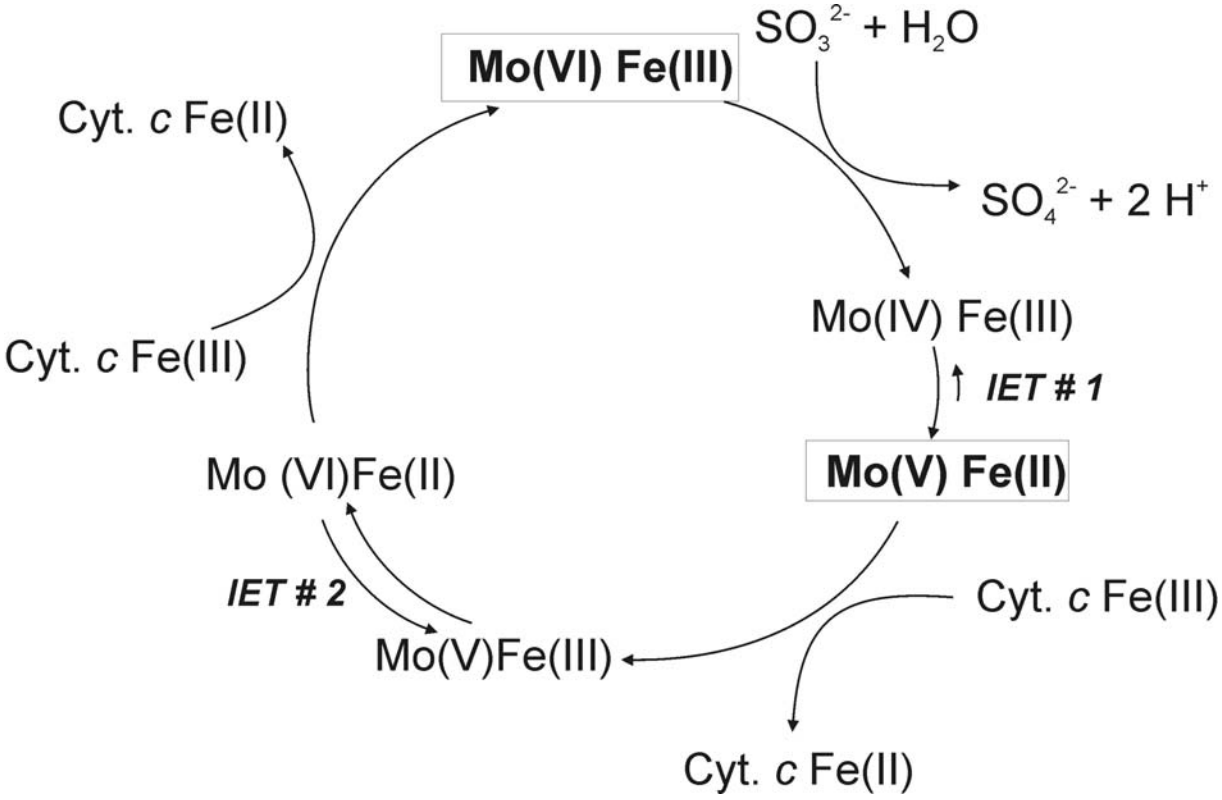
$SO_3^{2-} + H_2O$
Mo(VI) Fe(III)
Cyt. *c* Fe(II)
$SO_4^{2-} + 2\ H^+$
Mo(IV) Fe(III)
Cyt. *c* Fe(III)
IET # 1
Mo (VI)Fe(II)
Mo(V) Fe(II)
IET # 2
Cyt. *c* Fe(III)
Mo(V)Fe(III)
Cyt. *c* Fe(II)

Figure 2

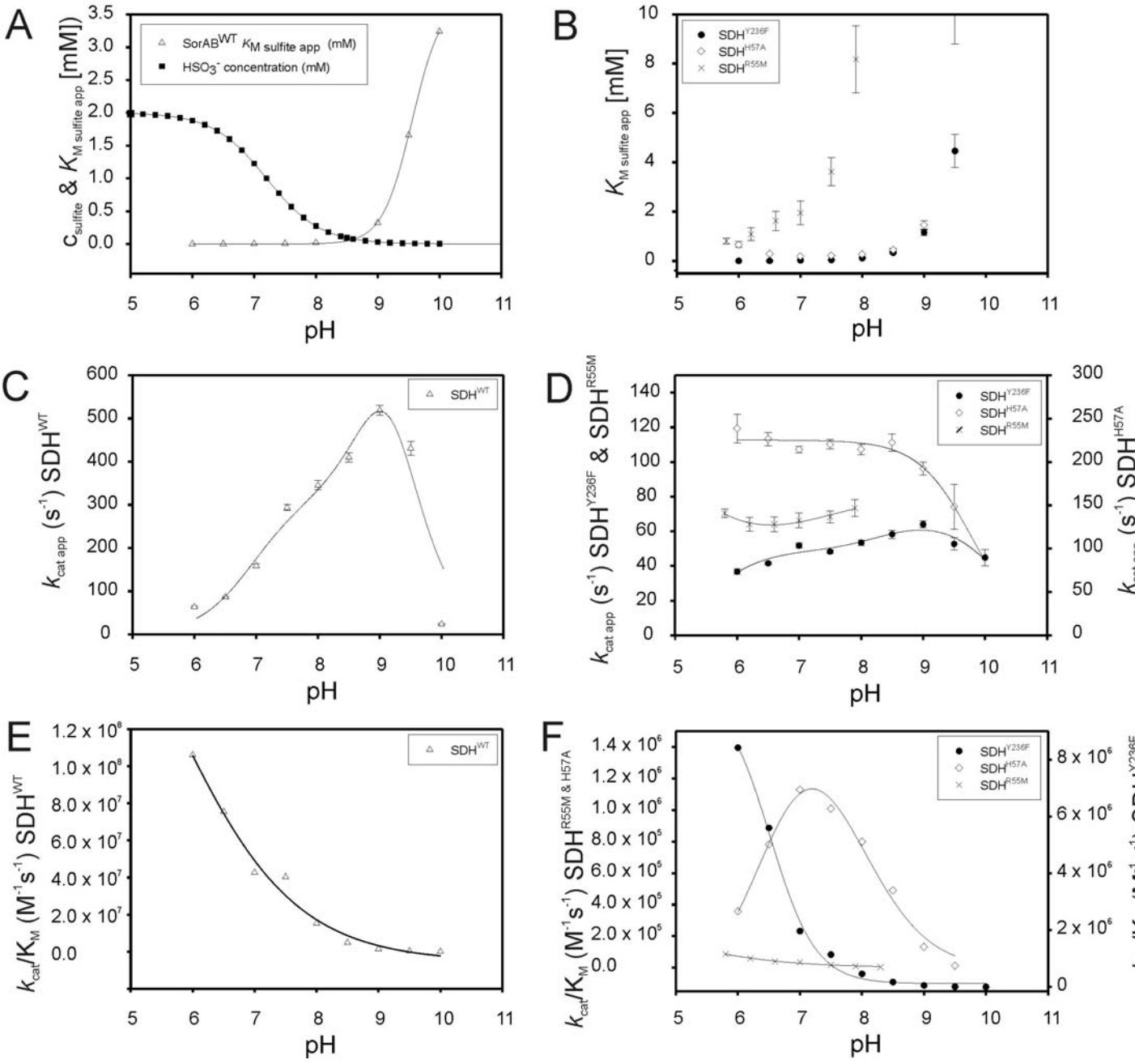
A
B
C
D
E
F
pH
SorAB^WT K_M sulfite app (mM)
HSO3- concentration (mM)
SDH^Y236F
SDH^H57A
SDH^R55M
SDH^WT
c_sulfite & K_M sulfite app [mM]
K_M sulfite app [mM]
k_cat app (s-1) SDH^WT
k_cat app (s-1) SDH^Y236F & SDH^R55M
k_cat app (s-1) SDH^H57A
k_cat/K_M (M-1s-1) SDH^WT
k_cat/K_M (M-1s-1) SDH^R55M & H57A

Figure 3

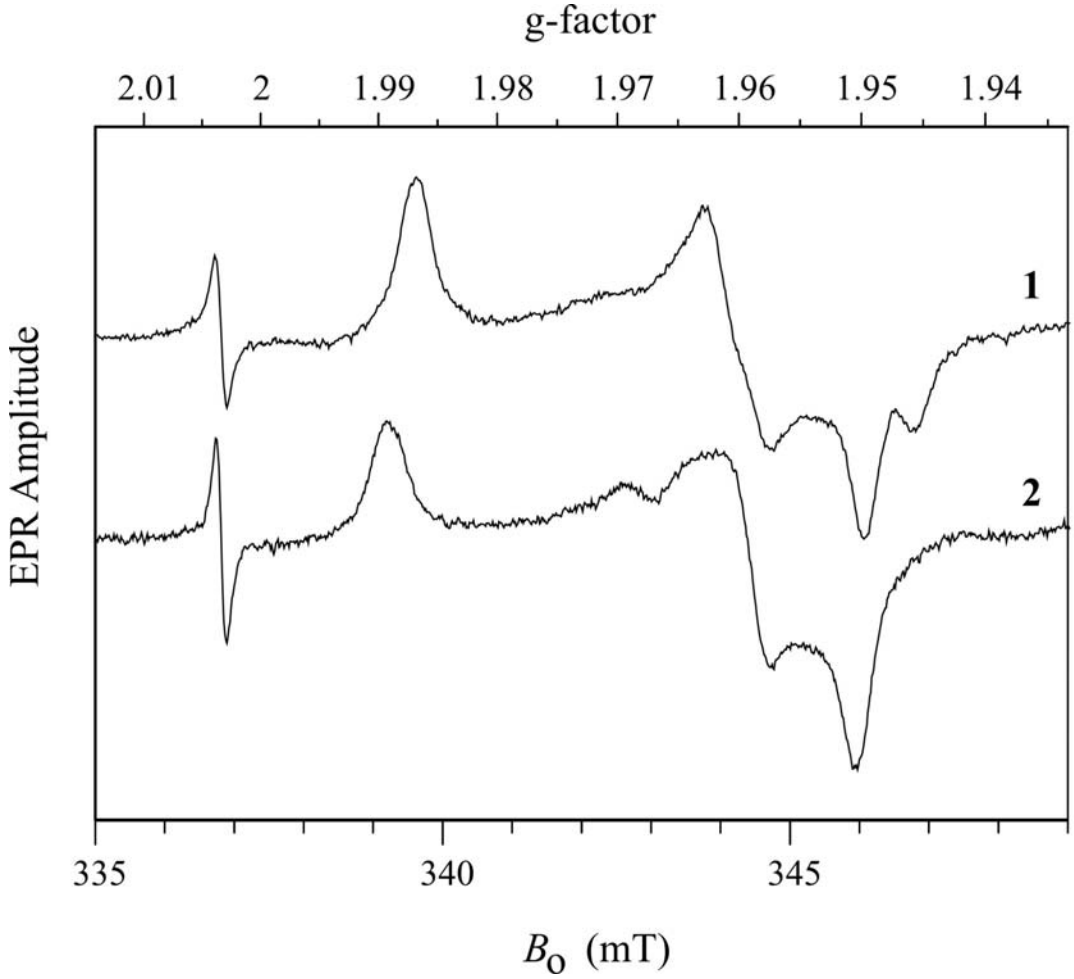
g-factor
2.01
2
1.99
1.98
1.97
1.96
1.95
1.94
EPR Amplitude
1
2
335
340
345
B_o (mT)

Figure 4

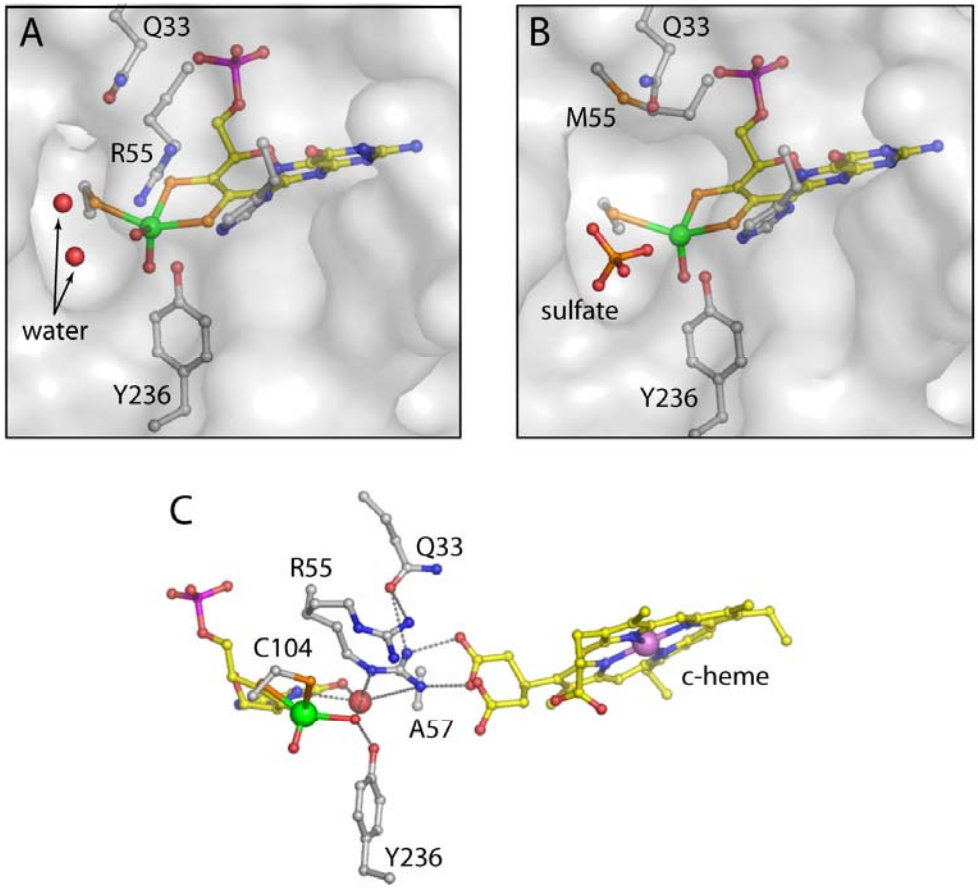
A
Q33
R55
water
Y236
B
Q33
M55
sulfate
Y236
C
Q33
R55
C104
A57
c-heme
Y236

Figure 5

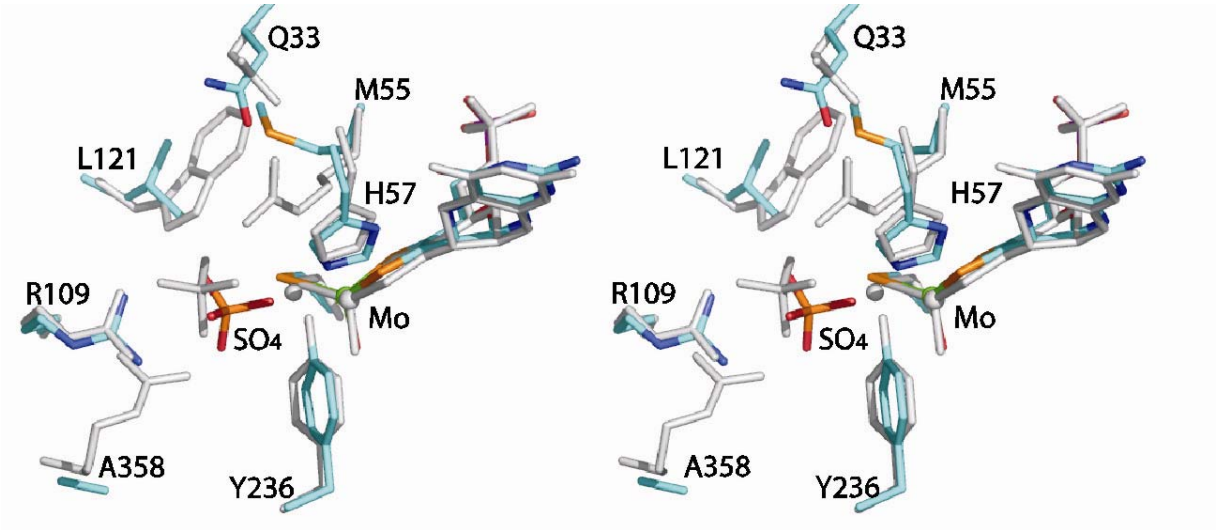
Q33
M55
L121
H57
R109
SO4
Mo
A358
Y236
Q33
M55
L121
H57
R109
SO4
Mo
A358
Y236

Figure 6

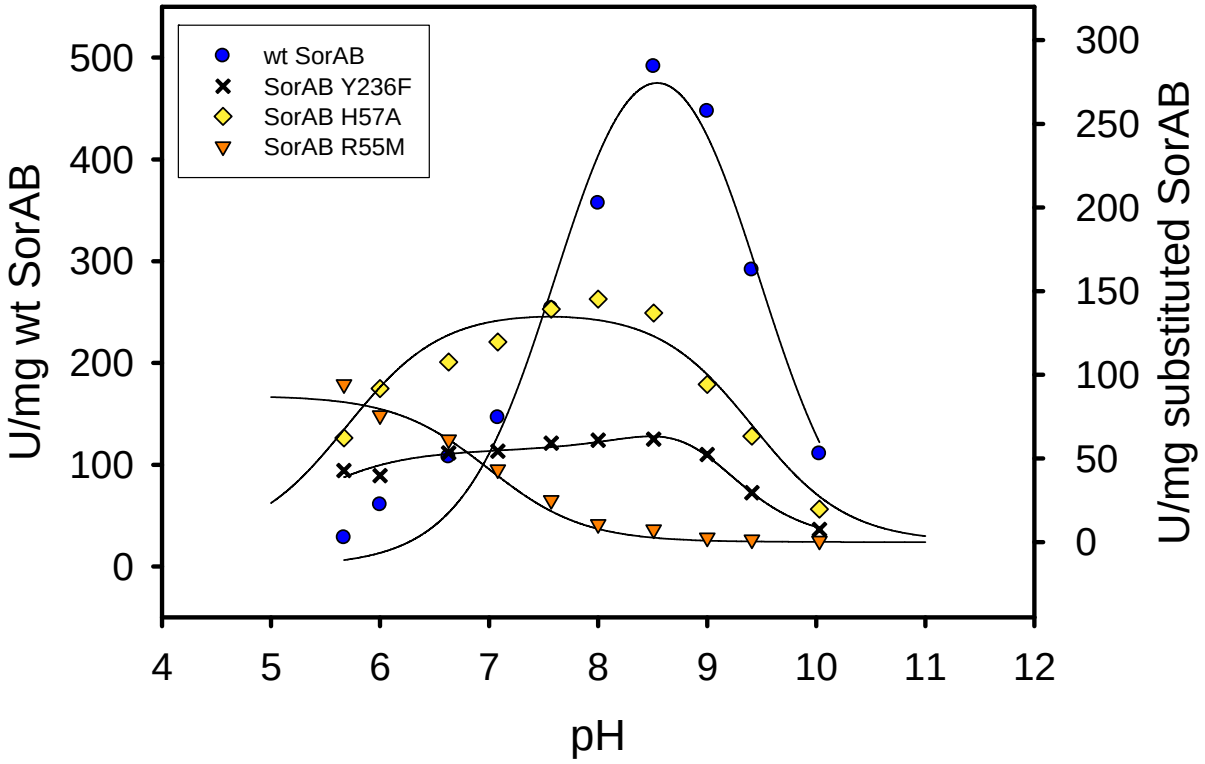
wt SorAB
SorAB Y236F
SorAB H57A
SorAB R55M
U/mg wt SorAB
U/mg substituted SorAB
pH
0
100
200
300
400
500
0
50
100
150
200
250
300
4
5
6
7
8
9
10
11
12

Figure S1

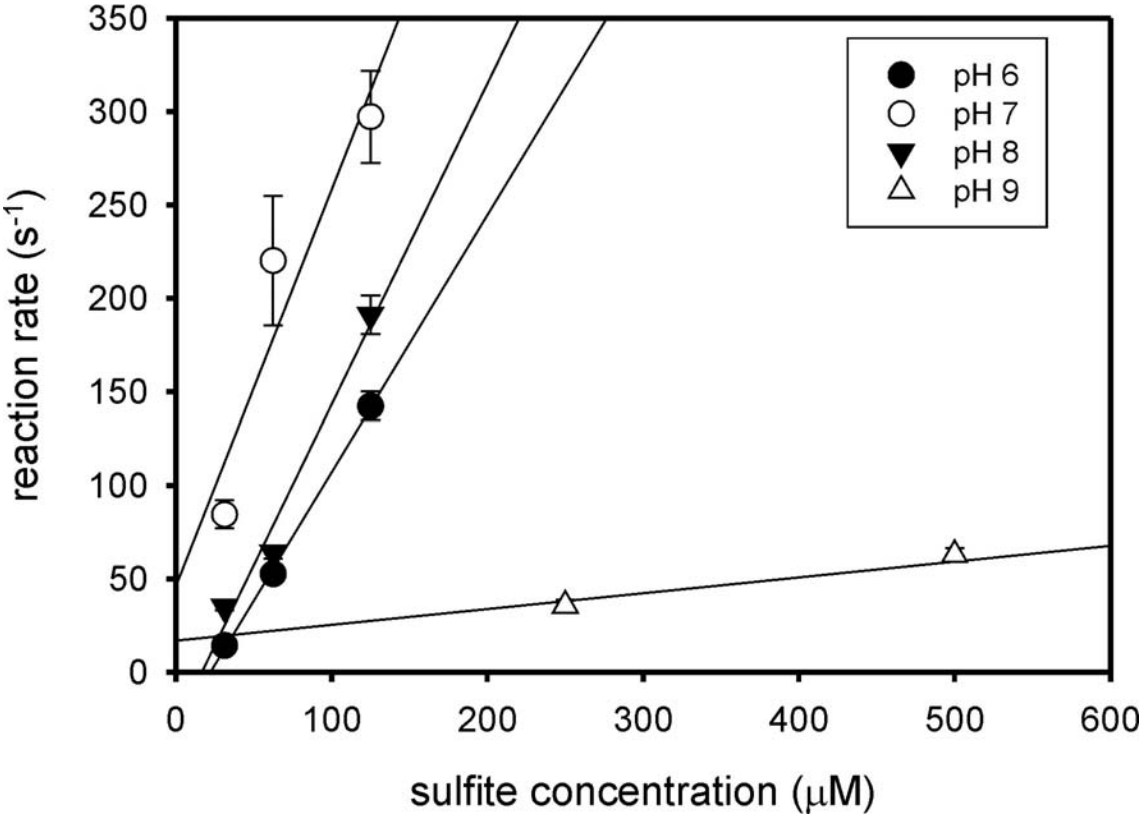
reaction rate (s-1)
sulfite concentration (μM)
pH 6
pH 7
pH 8
pH 9
0
50
100
150
200
250
300
350
0
100
200
300
400
500
600

Figure S2

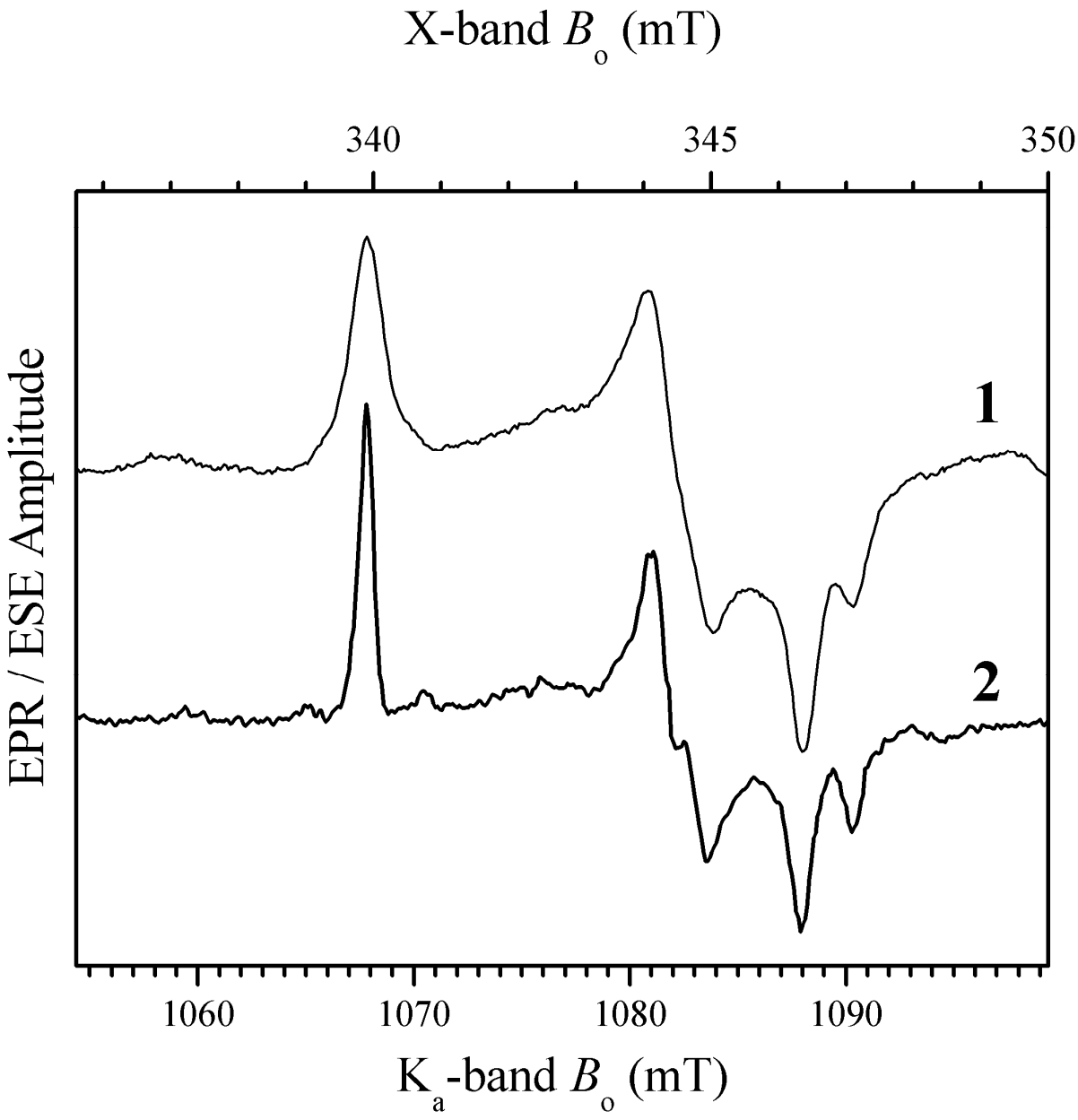
X-band B_o (mT)
340
345
350
EPR / ESE Amplitude
1
2
1060
1070
1080
1090
K_a-band B_o (mT)

Figure S3

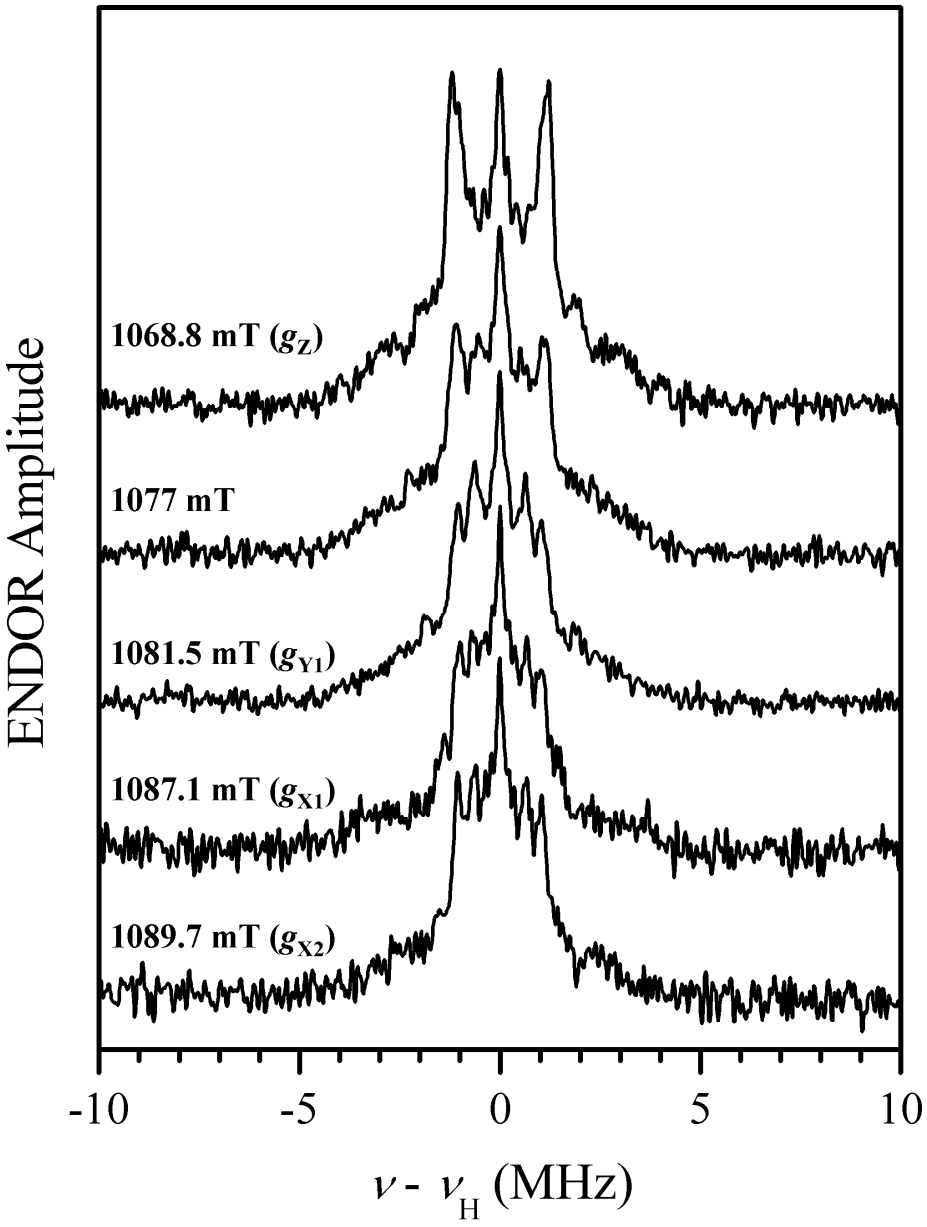
ENDOR Amplitude
1068.8 mT (g_Z)
1077 mT
1081.5 mT (g_{Y1})
1087.1 mT (g_{X1})
1089.7 mT (g_{X2})
-10
-5
0
5
10
ν - ν_H (MHz)

Figure S4

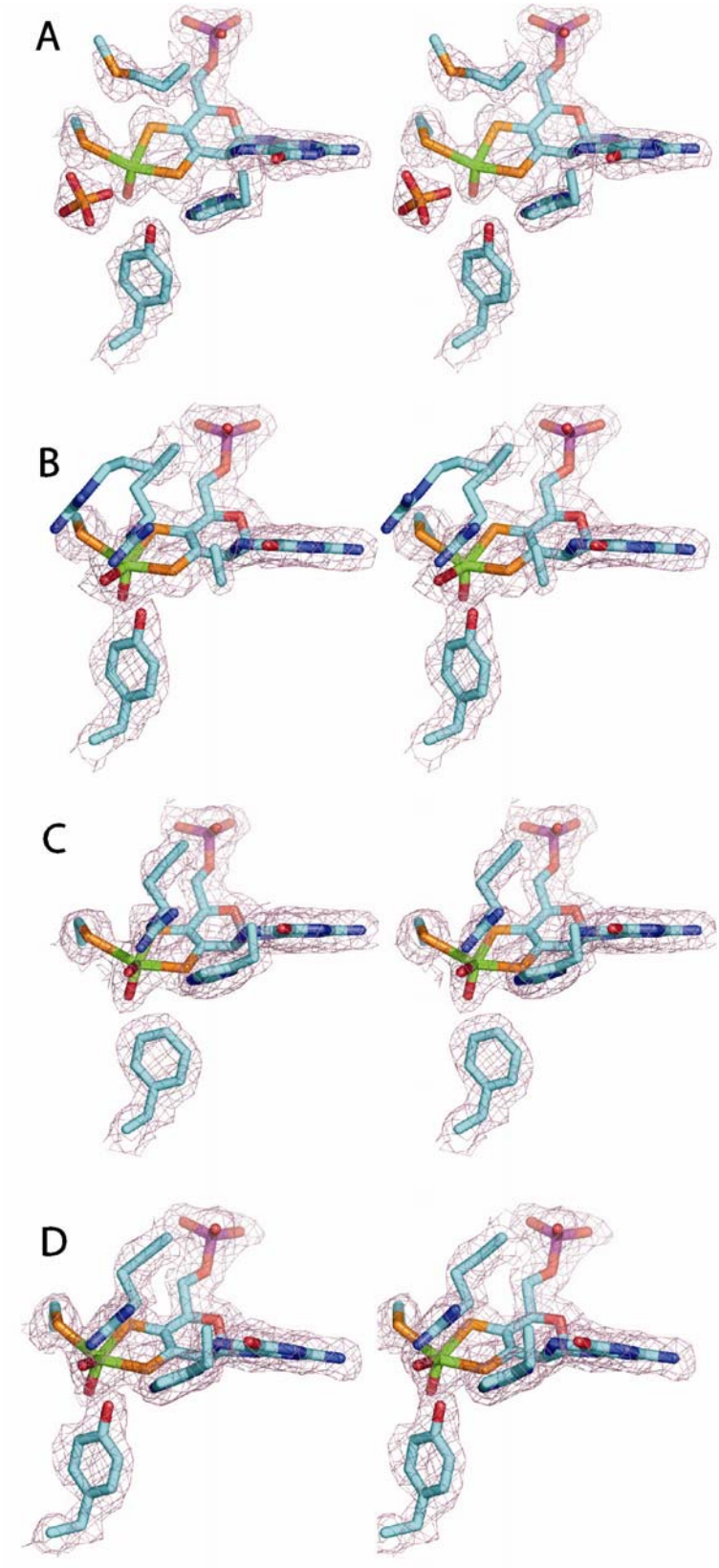

Figure S5